# Computer-aided detection of wall motion abnormalities in cardiac MRI

Suinesiaputra, A.

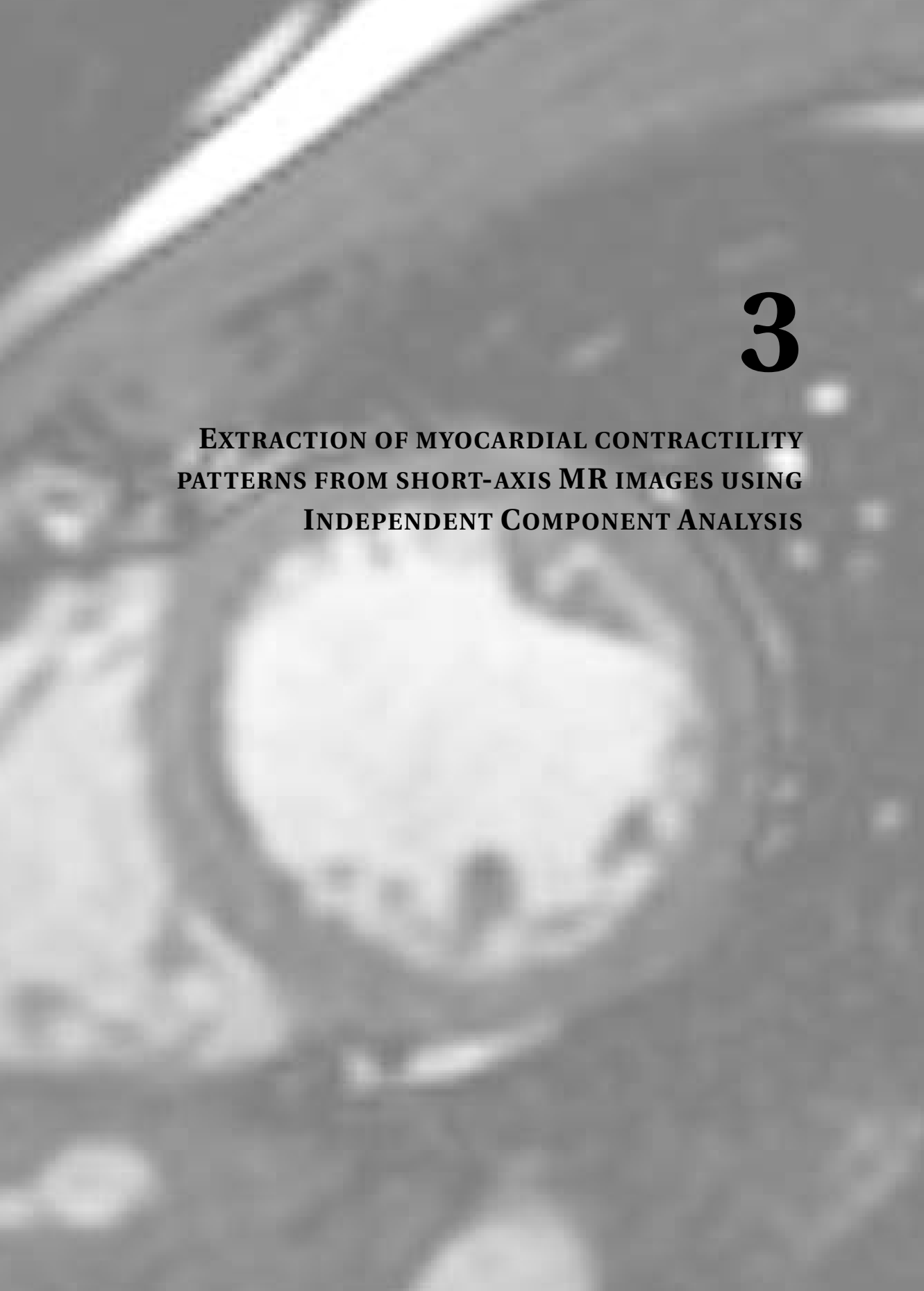

# 3

# Extraction of myocardial contractility patterns from short-axis MR images using Independent Component Analysis

**Abstract**

Regional wall motion analysis has been used in clinical routine to assess myocardial disease, particularly in ischaemia. This disease can be distinguished from normals by looking at the local abnormality of cardiac motion. In this chapter, the first result of a feature extraction experiment using Independent Component Analysis (ICA) is presented, where abnormal patterns of myocardial contraction from patients are recognizable and distinguishable from normal subjects.

This chapter was adapted from:
A. Suinesiaputra, A. F. Frangi, M. Üzümcü, J. H. C. R. Reiber, and B. P. F. Lelieveldt. Extraction of myocardial contractility patterns from short-axis MR images using independent component analysis. In M. Sonka, I. A. Kakadiaris, and J. Kybic, editors, *Computer Vision and Mathematical Methods in Medical and Biomedical Image Analysis*, volume 3117 of *Lecture Notes in Computer Science*, pages 75–86. Springer, 2004.

There are things we know that we know. There are known unknowns. That is to say there are things that we now know we don't know. But there are also unknown unknowns. There are things we don't know we don't know.

NATO Press Conference, 6 June 2002
DONALD RUMSFELD

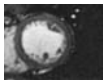



MYOCARDIAL contractility is an important quantitative indicator for the diagnosis of myocardial diseases. This function can be visually examined and quantified by using a cine MRI sequence. Two most important phases for myocardial contraction are the *end-diastole* (ED), or the start of contraction, and the *end-systole* (ES), or the end of contraction.

Abnormal myocardial contraction is mainly caused by the occlusion of coronary arteries. Coronary artery occlusion causes the imbalance of oxygen supply to the heart which triggers the so-called *ischaemic events* starting from perfusion abnormalities, wall motion abnormalities and finally myocardial infarction. Figure 3.1 shows two examples of MRI images from a healthy volunteer and an infarct patient, both at ES phase. Note that the inferior region (indicated by a white arrow) of the infarct patient does not contract. This region has a small wall thickness value.

To extract myocardial contractility patterns, shape decomposition technique is applied through subspace analysis. Subspace analysis techniques have been used in many areas, including appearance-based modeling and recognition. Principal Component Analysis (PCA) is the common subspace analysis for dimensionality reduction. Independent Component Analysis (ICA) is another subspace analysis, which seeks statistically independent components of the observed data. ICA is commonly used for blind source separation of an observed signal.

In machine learning, both PCA and ICA can be used for feature extraction [1–3]. There exists some literature showing a comparison between both methods with different results. Moghaddam [4] shows no statistical differences between PCA and ICA. Draper et al. [5] compared ICA and PCA for face recognition and reported that some ICA algorithms give better performance than PCA, but some do not.

Regardless of these comparisons, PCA and ICA are both linear generative models, because every training shape can be approximated by a linear combination of the components. An important difference between ICA and PCA lies in the shape variation. Independent components from ICA create local shape variation, while principal components from PCA give a global shape variation [6]. This indicates that ICA is more suitable for extracting local shape features compared to PCA. Local feature extraction is a desirable property specifically in this study.

In this chapter, an ICA-based local feature extraction method for the diagnosis of myocardial disease is presented, especially for myocardial infarction. Section 3.1 describes the myocardial shape model, the ICA method and a new sorting method for ICA modes. Section 3.2 presents experimental results, followed by a discussion in Section 3.3.

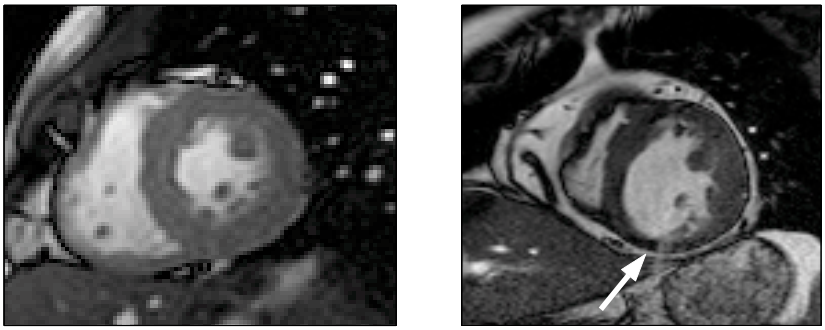

(a) healthy volunteer (b) infarct patient

FIGURE 3.1: MRI images of a healthy volunteer and an infarct patient at end-systole (the final contraction phase in the cardiac cycle). White arrow points to the infarcted tissue of the patient, where that myocardial region has a small contraction.

## 3.1 Methodology

### 3.1.1 ICA model

In this study, the observation data are left ventricular (LV) myocardial contours, manually drawn from short-axis cardiac MR images at ED and ES phases. Samples for each observation are landmark points, defined by equal angular distance along each contour.

To model the contractility pattern between ED and ES, contours for each subject are combined serially into one *shape* vector. A shape $\mathbf{x} \in \mathbb{R}^{2m}$ is defined by $m$ landmark points from 4 contours together in the following order: endocardium (inner) contour at ED, epicardium (outer) contour at ED, endocardium contour at ES and epicardium contour at ES. Thus the shape analysis is performed on all concatenated contours together, preserving the aspect ratio between ED and ES. This keeps the contractility patterns among different subjects (shapes).

The shape vector $\mathbf{x}$ consists of $m$ pairs of $(x, y)$ coordinates of landmark points:

$$\mathbf{x} = \left(x_1, y_1, x_2, y_2, \ldots, x_m, y_m\right)^T \tag{3.1}$$

The mean shape $\bar{\mathbf{x}}$ from $n$ shapes is defined by

$$\bar{\mathbf{x}} = \frac{1}{n} \sum_{i=1}^{n} \mathbf{x}_i \tag{3.2}$$

Each observed data (shape) $\mathbf{x}$ can be generated by a linear combination of a component matrix $\Phi \in \mathbb{R}^{2m \times p}$. This linear generative model is formulated as follows

$$\mathbf{x} \approx \bar{\mathbf{x}} + \Phi \mathbf{b}, \tag{3.3}$$

where $\bar{\mathbf{x}}$ is the mean shape and $\mathbf{b} \in \mathbb{R}^p$ is the component weighting vector.

In ICA, the basis of the subspace is sought to be statistically independent, with the main assumption of the non-gaussian distribution of the observed data [7]. The resulting subspace is non orthogonal and unordered. There is no closed form solution for ICA. Several numerical algorithms to estimate ICA are available (see [8] for the survey of ICA algorithms).

When applied to shape modeling, there is an important property of ICA in its *modes*. As the number of computed independent components increases, the component gives more localized shape variations. On the contrary, if the number of independent components is too small, then the component gives global shape variation, much like PCA modes. A shape variation in ICA has a general shape of a local bump, whereas the remainder of the shape is unaffected (see Figure 3.2(a)). This is the difference between ICA and PCA: PCA modes give global shape variations, distributed over the entire contour (see Figure 3.2(b)). Üzümcü et. al. [6] have presented the comparison between PCA and ICA in the modelling of cardiac shapes.

### 3.1.2 Geometry-based sorting for ICA modes

In subspace analysis, the number of selected components is usually less than the dimension of the observed data. This allows a lower dimensional representation that still covers enough information of the observed data, either for description, detection or recognition.

Principal components are ordered from higher variance to the lowest, making it straightforward to select which and how many components to retain for further analysis; this is however not the case in ICA. There is no natural sorting criteria for independent components. One needs to define a sorting method for independent components that is suitable for a specific application. Since ICA components are local, they can be sorted based on their local position along the contour and this sorting criterion gives a more intuitive interpretation of local shape variations.

Let $i$th mode $\hat{\mathbf{x}}_i$ be defined as the shape variation at the $i$th column of $\Phi$:

$$\hat{\mathbf{x}}_i = \bar{\mathbf{x}} + \Phi \mathbf{e}_i \tag{3.4}$$

where $1 \leq i \leq p$ and $\mathbf{e}_i \in \mathbb{R}^p$ is a vector that has element 1 at the $i$th position whereas the rest are 0. Thus, $\hat{\mathbf{x}}_i$ describes the $i$th mode of shape variation.

To locate the position of each $\hat{\mathbf{x}}_i$ along a contour, a bank of Gaussian filters were applied and then followed by the normalized cross-correlation of each of the filters with a *distance vector* of each mode $\hat{\mathbf{x}}_i$. The $i$th mode distance vector $\mathbf{d}_i \in \mathbb{R}_+^m$ is defined as the distance of each landmark point in the shape variation $\mathbf{x}_i$ to the mean shape. Each element $j$ of the $i$th distance vector is defined by

$$\mathbf{d}_i^{(j)} = \sqrt{\sum_{k=2j-1}^{2j} \left( \hat{\mathbf{x}}_i^{(k)} - \bar{\mathbf{x}}^{(k)} \right)^2}, \tag{3.5}$$

where $j = 1, 2, \ldots, m$. The cross-correlation is performed only on a particular contour, circularly. Thus there are four cross-correlation processes, because there are four contours for each shape.

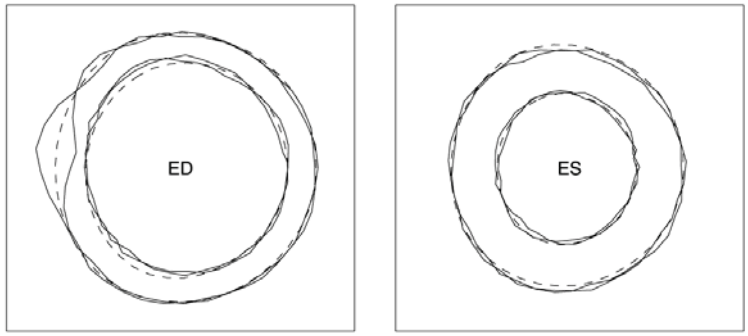


(a) ICA mode (variation is at ED-epi)

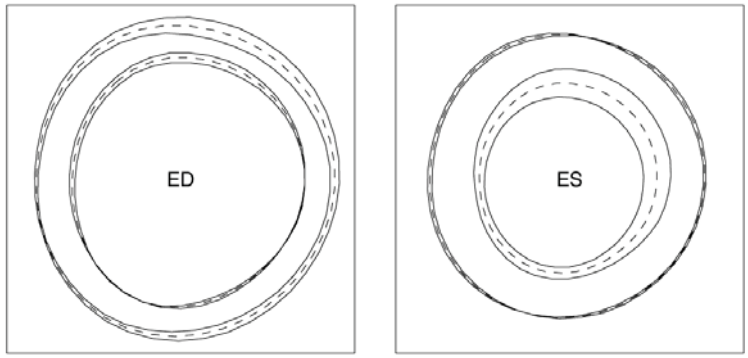


(b) The first PCA mode

FIGURE 3.2: Examples of local shape variation from an ICA mode. As a comparison, the first PCA mode is given. The mean shape is shown with dashed lines. The solid lines are modes of shape variation.

The Gaussian filter giving the maximum cross-correlation for vector $\mathbf{d}_i$ is stored. The center of this filter defines the position of the i-th component; the width of the Gaussian filter represents the width of the component. Figure 3.3(a) shows an example of the cross-correlation response from a component.

There is an extra advantage of using the normalized cross-correlation for sorting ICA modes. Modes that consist of noise are automatically detected and thus can be eliminated. Noise modes have a global wrinkled shape variation along the whole contour, which correlates best with the widest Gaussian filter. Figure 3.3(b) shows an example of the cross-correlation response for a noise component. After all modes have been cross-correlated, positions of all modes are determined. Subsequently, ICA modes are sorted based on position along the contour.

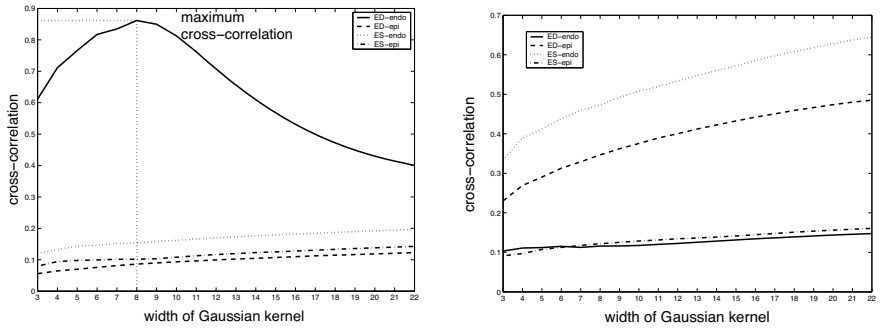


(a) a component (b) a noise component

FIGURE 3.3: Example of maximum cross-correlation results from two components.

### 3.1.3 Cluster measurement metrics

To evaluate the cluster formation between normal and patient subjects, a number of $q$ components ($q \leq p$) are selected from the weighting coefficient matrix $\mathbf{b}$.

Let $\mathfrak{D} = \sum_i^c \mathfrak{D}_i \subset \mathbb{R}^q$ be a subset of the weighting coefficient matrix $\mathbf{b}$, after $q$ components are selected. Let $c$ be the number of classes. In this case, $c = 2$, because there are only two classes, i.e. normals and patients.

The first measurement is called *within-cluster scatter matrix*, which measures the compactness of a cluster. The within-cluster scatter matrix $\mathbf{S}_W$ is defined as the sum of scatter matrices for each group:

$$\mathbf{S}_W = \sum_{i=1}^{c} \sum_{\mathbf{x} \in \mathfrak{D}_i} (\mathbf{x} - \mathbf{m}_i)(\mathbf{x} - \mathbf{m}_i)^T, \tag{3.6}$$

where $\mathbf{m}_i$ is the mean ("center of gravity") of the cluster $i$.

A scalar value representing the measurement of the compactness from this metric is simply its trace. The trace of a scatter matrix accounts for the square of the scattering radius, because it is actually the sum of the variances in each coordinate direction. This scalar value is equal to the sum-of-squared error. Thus one seeks the minimum of this value to get the best representation of a cluster. The compactness measurement $J_W$ can be defined as follows

$$J_W = \text{tr}[\mathbf{S}_W] \tag{3.7}$$

The second measurement is *between-cluster scatter matrix* measurement $\mathbf{S}_B$, which represents how far clusters are separated. It is defined as follows

$$\mathbf{S}_B = \sum_{i=1}^{c} n_i \, (\mathbf{m}_i - \mathbf{m})(\mathbf{m}_i - \mathbf{m})^T, \tag{3.8}$$

where $n_i$ is the number of subject of the $i$th cluster and $\mathbf{m}$ is the total mean:

$$\mathbf{m} = \frac{1}{n} \sum_{\mathbf{x} \in \mathfrak{D}} \mathbf{x} \tag{3.9}$$

The scalar measurement value of the between-cluster scatter matrix is also its trace:

$$J_B = \mathrm{tr}[\mathbf{S}_B] \tag{3.10}$$

The within-cluster and between-cluster scatter matrices are mostly used to design cluster validity indices for clustering methods [3]. In this study, these measurements are used to compare the quality of the cluster representation given by PCA and ICA components.

To visualize the cluster distribution, the Fisher discriminant line [3] is calculated and coefficient values from the selected components are projected to the Fisher line. Fisher linear discriminant accounts the ratio between the between-cluster and the within-cluster matrix measurements and it is given by:

$$\mathbf{w} = \mathbf{S}_W^{-1} (\mathbf{m}_1 + \mathbf{m}_2), \tag{3.11}$$

where $\mathbf{w}$ is a vector with the direction that maximizes the separation between the two clusters $\mathbf{m}_1$ and $\mathbf{m}_2$.

## 3.2 Experimental results

Forty-two normal subjects and forty-seven patients suffering from myocardial infarction were investigated. For each subject, endocardial and epicardial contours at ED and ES phases from short-axis view MRI were drawn manually by experts.

All contours were resampled to 40 landmarks defined by equi-angular sampling, starting from the intersection point between the lower right ventricular myocardium with the left ventricular myocardium. The total number of landmark points for each shape were 160 points.

ICA calculation was performed by using the JADE algorithm [9], implemented in Matlab (Matlab v7.0, The Mathworks, Natick, MA, USA). The number of ICA modes was selected carefully to 40 in this study, that gives enough local shape variations for each of the four contours. If the number is too small, then the shape variations become more global. If the number is too large, then too many local shape variations may occur, which look like noise components.

For the ICA mode sorting, 20 Gaussian filters were used, ranging from width 3 to 22. Modes correlating with a Gaussian filter, which has width larger than 20 (half of a contour), were considered to be noise. From the original 40 ICA modes, the sorting method retained 35 modes, thus eliminated 5 noise modes.

### 3.2.1 Weighting coefficient matrix

Figure 3.4(a) shows the weighting matrix $\mathbf{b}$ of the ICA model that is constructed from shapes of normal subjects and infarct patients. The weighting coefficient matrix contains values that are needed to generate each training shape. These coefficient values

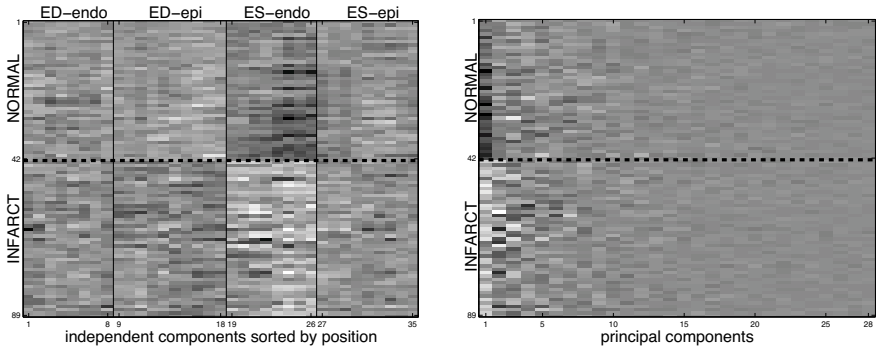


(a) ICA model

(b) PCA model

FIGURE 3.4: The weighting coefficient between normal subjects and infarct patients.

are different for each subject. Thus the weighting matrix **b** is the most important value for classification purposes.

From Figure 3.4(a), the boundary between normal and patient subjects is clearly distuingishable in the endocardium at the ES phase. As a comparison, Figure 3.4(b) shows the PCA model from the same data. With PCA, the difference between the two groups is less pronounced. It is clearly visible only from the first component.

### 3.2.2 Mean cluster distance

To enable the comparison between PCA and ICA, the weighting coefficient matrices for both models are normalized, such that $||\mathbf{b}|| = 1$. Hence weighting coefficient matrices for PCA and ICA are both in the same unit.

The distance between means of normal and patient subjects for each component is calculated using the *mean cluster distance* (MCD), as given by:

$$d_i = |\mathbf{m}_{n,i} - \mathbf{m}_{p,i}|, \tag{3.12}$$

where $i$ is an index of a component, $m_{n,i}$ and $m_{p,i}$ are the mean of the weighting coefficient values at the $i$-th component for normal and patient subjects respectively. Figure 3.5 shows the bar plot of the MCD of PCA and ICA for each mode.

A t-test experiment was conducted on each of independent and principal component to see whether the two means from normal and patient coefficient values come from two different clusters. The result is illustrated in Figure 3.5. From 35 selected independent components, there are 27 components with each has statistically significant difference of two means, while PCA only gives 1 component (the first principal component). The t-tests were performed with 95% confidence interval.

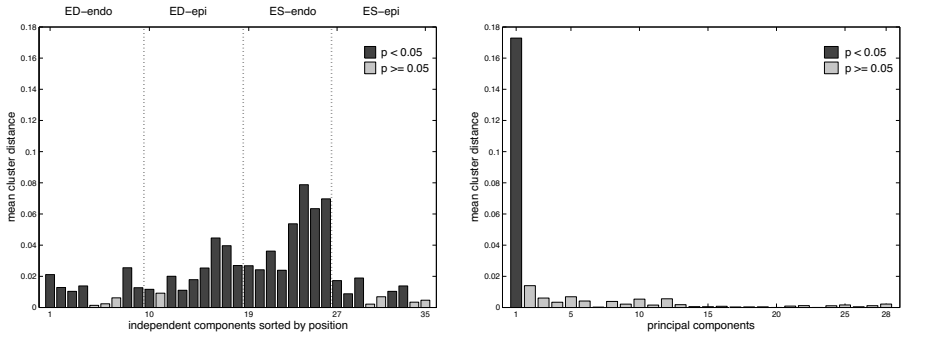


(a) ICA (b) PCA

FIGURE 3.5: Mean cluster distance of each component from ICA and PCA. The results of t-test experiment on each component are shown as dark gray for $p < 0.05$ and light gray bars for $p \geq 0.05$.

It is evident that independent components at ES-endo are among the highest MCD value. Mean cluster distance of the first PCA mode is the highest among others, even compared with ICA.

### 3.2.3 Cluster analysis

In this study, only an analysis of cluster properties are presented, but **not yet** a classification result. Clusters are defined by selecting all independent components from ICA and principal components that covers 95% of total variance from PCA. This gives 35 ICA components and 16 PCA components.

Table 3.1 shows the measurement results using (3.7) for the cluster compactness and (3.10) for the cluster separation. Figure 3.6 shows result of the projected coefficient values to their Fisher discriminant line.

PCA gives better compactness than ICA, but less separable (see Table 3.1). However the projection to the Fisher discriminant line favors ICA (see Figure 3.6). There is only one point of misclassification in ICA, if a threshold value is defined. However there are more overlaps in the projection of principal components to the Fisher discriminant line.

TABLE 3.1: Cluster validity measurement results.

| | compactness ($J_W$) | separation ($J_B$) |
|---|---|---|
| ICA | 1.84 | 0.66 |
| PCA | 0.65 | 0.12 |


FIGURE 3.6: Projection of independent components (above) and principal component (below) to their Fisher discriminant line.

### 3.2.4 Separation degree

The MCD in (3.12) can be used to map the cluster separation for each component onto the same information for each landmark points. This enables a more intuitive regional interpretation of the differences between the two groups.

From the sorting of independent components, location and width of each component are retrieved. Thus the corresponding Gaussian function for each component can be generated and multiply it with its MCD, resulting a Gaussian mixture for each landmark point. The sum of the Gaussian mixture is called *separation degree*. Figure 3.7(a) shows the separation degree of the ICA model from normal and patient subjects. Figure 3.7(b) also shows the same visualization, but a more intuitive way using the bullseye plot, where the color denotes the separation degree.

Figure 3.7(b) corresponds with Figure 3.4(a), where the most important feature to distinguish between normal and patient is the endocardium at ES phase. The least important features lie on the epicardium contour at ES phase, where there is a small separation degree.

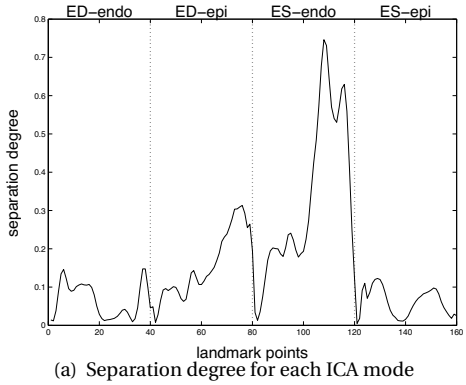


(a) Separation degree for each ICA mode

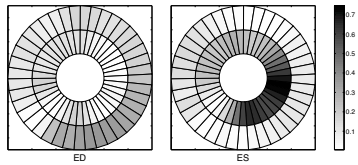


(b) Bullseye plot of the separation degree. The inner wall is endo-contour and the outer is epi-contour.

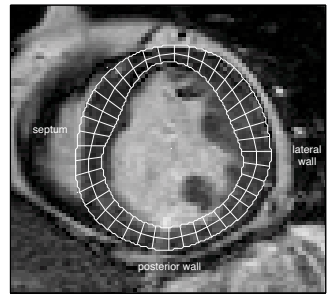


(c) An illustration of the bullseye plot interpretation in the short-axes MRI.

FIGURE 3.7: The separation degree of the ICA model between normal subjects and infarct patients.

## 3.3 Discussion

The potential of ICA in the computer-aided diagnosis of myocardial diseases has been investigated. The first result indicates that the ICA method is a promising analysis tool to extract local shape deformations from observed data. The sorting method of independent components based on their position leads to an anatomically meaningful interpretation for classification purposes. The weighting coefficient matrix from the ICA model can clearly distinguish between the two different groups in the endo-contour at ES.

From the cluster analysis, projection of independent components to the Fisher discriminant line gives better cluster representation than principal components. Given the ability to classify globally and to extract local features, ICA is a powerful tool to detect and to localize shape abnormalities, comparing favorably to PCA.

The experimental results revealed that most of the infarction area affects the endocardium in the infero-lateral wall, because the data contains most patients who have infarction in the lateral and inferior regions. A few patients have infarction in the septum area. From this study, the endocardium at end-systole phase is the most distinguishable feature, because this is the part of myocardium having the most deformation process due to contraction.

The reason why classification was not performed in this experiment is that the problem of classifying a patient versus normal is a toy problem. In clinical routine, it is not interesting to determine a subject as a patient. It is more important to detect if there is an anomaly, to localize it and then to quantify the disease.

The number of computed independent components is a free parameter to choose. The smaller the number is, the more global the independent components are for a shape variation. On the other hand, the shape variation becomes more localized if this parameter is increased. Thus a method to find an optimal number of independent components is needed. An analysis of how sensitive this parameter is to the diagnostic performance in this case will be helpful to define the optimal value.

The next important clinical question for the diagnosis of myocardial infarction is at which particular region of myocardium a patient has an infarction. This basically to localize the local abnormality and to quantify the severity of the disease.

## 3.4 References


[1] M. S. Bartlett, J. R. Movellan, and T. J. Sejnowski, "Face recognition by Independent Component Analysis," *IEEE Trans. on Neural Networks*, vol. 13, no. 6, pp. 1450–1464, Nov. 2002.

[2] T.-W. Lee, M. S. Lewicki, and T. J. Sejnowski, "ICA mixture models for unsupervised classification of non-Gaussian classes and automatic context switching in blind signal separation," *IEEE Trans. Pattern Anal. Mach. Intell.*, vol. 22, no. 10, pp. 1078–1089, 2000.

[3] R. O. Duda, P. E. Hart, and D. G. Stork, *Pattern Classification*, 2nd ed. John Wiley & Sons, Inc., 2001.

[4] B. Moghaddam, "Principal manifolds and probabilistic subspaces for visual recognition," *IEEE Trans. Pattern Anal. Mach. Intell.*, vol. 24, no. 6, pp. 780–788, 2002.

[5] B. A. Draper, K. Baek, M. S. Bartlett, and J. R. Beveridge, "Recognizing faces with PCA and ICA," *Computer Vision and Image Understanding*, vol. 91, no. 1-2, pp. 115–137, 2003.

[6] M. Üzümcü, A. F. Frangi, J. H. Reiber, and B. P. Lelieveldt, "Independent Component Analysis in statistical shape models," in *Proc. of SPIE*, M. Sonka and J. M. Fitzpatrick, Eds., vol. 5032, May 2003, pp. 375–383.

[7] A. Hyvärinen and E. Oja, "Independent component analysis: algorithms and applications," *Neural Networks*, vol. 13, no. 4-5, pp. 411–430, 2000.

[8] A. Hyvärinen, "Survey on Independent Component Analysis," *Neural Computing Surveys*, vol. 2, pp. 94–128, 1999.

[9] J. Cardoso and A. Souloumiac, "Blind beamforming for non Gaussian signals," *IEEE Proceedings-F*, vol. 140, pp. 362–370, 1993.